

High-precision laser-assisted absolute determination of x-ray diffraction angles

K. Kubiček, J. Braun, H. Bruhns, J. R. Crespo López-Urrutia, P. H. Mokler et al.

Citation: [Rev. Sci. Instrum.](#) **83**, 013102 (2012); doi: 10.1063/1.3662412

View online: <http://dx.doi.org/10.1063/1.3662412>

View Table of Contents: <http://rsi.aip.org/resource/1/RSINAK/v83/i1>

Published by the [American Institute of Physics](#).

Related Articles

Comment on “Electron acceleration by a short laser beam in the presence of a long-wavelength electromagnetic wave” [J. Appl. Phys. **102**, 056106 (2007)]

[J. Appl. Phys.](#) **111**, 106102 (2012)

Enhancement in coupling efficiency from laser to forward hot electrons by conical nanolayered targets

[Appl. Phys. Lett.](#) **100**, 204101 (2012)

Note: A large aperture four-mirror reflective wave-plate for high-intensity short-pulse laser experiments

[Rev. Sci. Instrum.](#) **83**, 036104 (2012)

Time-resolved single-shot imaging of femtosecond laser induced filaments using supercontinuum and optical polarigraphy

[Appl. Phys. Lett.](#) **100**, 111107 (2012)

Multicolor Čerenkov conical beams generation by cascaded- $\chi(2)$ processes in radially poled nonlinear photonic crystals

[Appl. Phys. Lett.](#) **100**, 101101 (2012)

Additional information on Rev. Sci. Instrum.

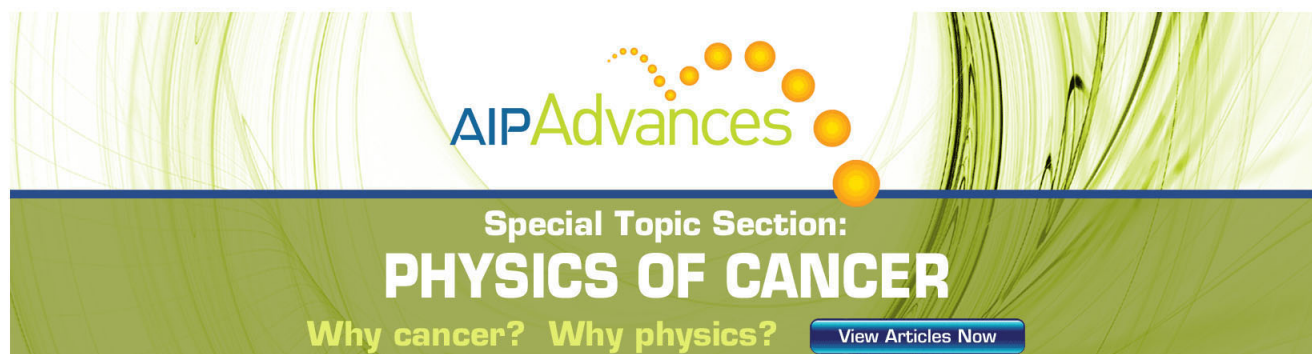
Journal Homepage: <http://rsi.aip.org>

Journal Information: http://rsi.aip.org/about/about_the_journal

Top downloads: http://rsi.aip.org/features/most_downloaded

Information for Authors: <http://rsi.aip.org/authors>

ADVERTISEMENT

The advertisement features a green and yellow abstract background with wavy lines. At the top, the text 'AIPAdvances' is displayed in a green, sans-serif font, with a series of orange dots of varying sizes arranged in a curved path above it. Below this, the text 'Special Topic Section:' is in a smaller, white, sans-serif font, followed by 'PHYSICS OF CANCER' in a large, bold, white, sans-serif font. At the bottom, the text 'Why cancer? Why physics?' is in a yellow, sans-serif font. To the right of this text is a blue button with the text 'View Articles Now' in white.

High-precision laser-assisted absolute determination of x-ray diffraction angles

K. Kubiček,^{a)} J. Braun, H. Bruhns, J. R. Crespo López-Urrutia, P. H. Mokler, and J. Ullrich
Max-Planck-Institute for Nuclear Physics, D-69117 Heidelberg, Germany

(Received 4 July 2011; accepted 29 October 2011; published online 4 January 2012)

A novel technique for absolute wavelength determination in high-precision crystal x-ray spectroscopy recently introduced has been upgraded reaching unprecedented accuracies. The method combines visible laser beams with the Bond method, where Bragg angles (θ and $-\theta$) are determined without any x-ray reference lines. Using flat crystals this technique makes absolute x-ray wavelength measurements feasible even at low x-ray fluxes. The upgraded spectrometer has been used in combination with first experiments on the $1s2p\ ^1P_1 \rightarrow 1s^2\ ^1S_0$ w -line in He-like argon. By resolving a minute curvature of the x-ray lines the accuracy reaches there the best ever reported value of 1.5 ppm. The result is sensitive to predicted second-order QED contributions at the level of two-electron screening and two-photon radiative diagrams and will allow for the first time to benchmark predicted binding energies for He-like ions at this level of precision. © 2012 American Institute of Physics. [doi:10.1063/1.3662412]

I. INTRODUCTION

The precise knowledge of x-ray transition energies is the basis for a deep understanding of the structure of atoms and ions.^{1,2} The accuracy which can be achieved in high-precision crystal x-ray spectroscopy depends on the properties of the radiation source, the diffraction device and the detection system.³ For the absolute calibration of wavelengths two techniques can be taken: either wavelengths are measured relatively with respect to an absolutely known reference line or absolutely by geometrical means alone.

Among radiation sources, electron beam ion traps (EBITs) (Refs. 4–7) provide a very convenient technique to produce few-electron ions for high-precision wavelength measurements. In contrast to x-ray spectra obtained using the recoil-ion technique,^{8,9} the deceleration and electron capture method,¹⁰ or tokamak plasmas,¹¹ EBIT spectra are rather pure, in so far as coronal excitation conditions prevail, and therefore the lines are symmetric and satellite-free.¹² Conversely, it is also possible to prepare the otherwise disturbing satellite transitions also in a targeted way, using well-defined, monoenergetic excitation conditions.^{13,14} Moreover, EBIT spectral line positions are not affected by Doppler shifts on the level of accuracy achieved in x-ray crystal spectroscopy^{15–18} at accelerators.

In principle, several methods are available for precise x-ray wavelength determination: crystal spectroscopy, resonant laser spectroscopy, and bolometry. In general, resonant laser excitation, which in the optical region^{19–21} reaches extreme accuracies, would be the ideal spectroscopic tool. Unfortunately, throughout the last decades application of this method in the x-ray region suffered from the lack of appropriate laser sources. Only now, with x-ray free electron lasers (XFELs) being developed and starting operation at several places²² resonant laser fluorescence spectroscopy both in the vacuum

ultraviolet²³ and the x-ray region²⁴ up to photon energies of ~ 10 keV (Refs. 25–27) will become feasible.

Apart from that x-ray bolometers exhibit today a resolution near that of crystal spectrometers.^{28–32} Here, however, wavelengths can be measured relatively only.

Crystal spectrometers using curved^{33–37} or flat crystals are still used for high-resolution measurements of x-ray transition energies. The Bragg angle θ is typically determined with fractional uncertainties $\Delta\theta/\theta$ in the tens of ppm region relative to those of x-ray reference lines, e.g., K_α transition lines of copper, molybdenum, and tungsten,³⁸ by fixing the direction of incoming x-rays by collimating slits,³⁹ which unfortunately also reduces the x-ray flux. To avoid error contributions caused by the asymmetric reference lines, techniques without them were developed. Such methods include, for example, using a monolithic crystal, where two reflecting surfaces are separated by an accurately measured distance,⁴⁰ or the Bond method,⁴¹ where x-ray reflections at the Bragg angles θ and $-\theta$ are determined to eliminate errors due to a zero offset of the angular scale (double sided measuring technique).

Combining the Bond technique with a laser-assisted reference method for the precise directional determination of the incoming x-rays³ we have introduced a novel spectrometer type which we tested at the Heidelberg EBITs. Here laser beams are used as reference spots – called fiducials – instead of collimation slits.

In this review we report on a substantial upgrade of that combined concept, explicitly resolving curvatures of the x-ray lines on the two-dimensional detectors which previously were determined indirectly only. This improved the absolute accuracy by more than a factor of 10. In this new configuration the wavelength of the w -transition⁴² ($1s2p\ ^1P_1 \rightarrow 1s^2\ ^1S_0$) in He-like argon could be determined with an uncertainty of 1.5 ppm only. This result is the most precise value for a wavelength of any He-like ion reported so far, what makes it sensitive to binding energy QED contributions at the level of two-electron and two-photon radiative diagrams. Since various predictions

^{a)}Electronic mail: kubicek@mpi-hd.mpg.de.

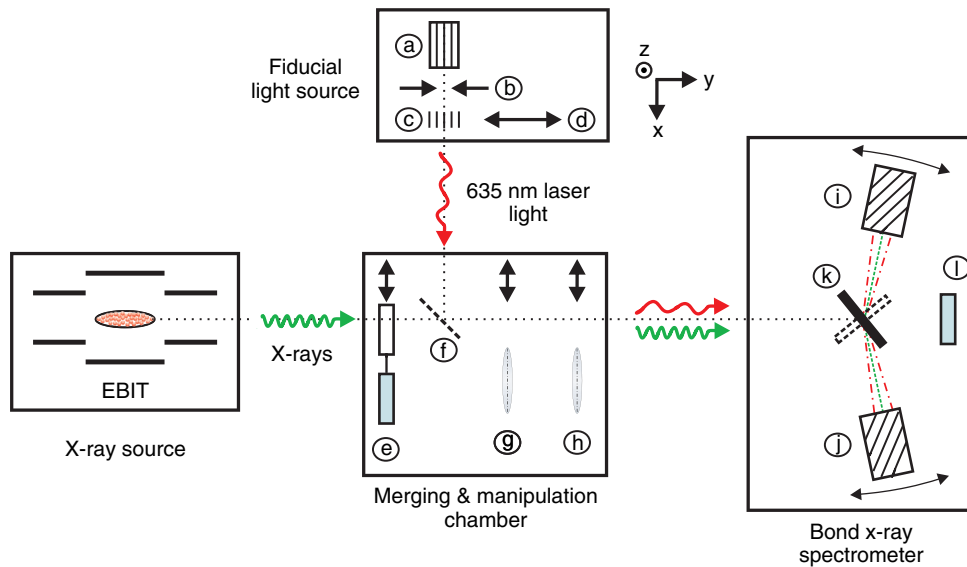


FIG. 1. (Color online) Schematic drawing of the x-ray spectrometer arrangement coupled to the Heidelberg EBIT. *X-ray source*: EBIT in parallel (shown) or perpendicular (head on) arrangement with respect to the crystal rotation axis. *Fiducial light source* (generation of light fiducials): (a) denotes the laser source, (b) a pinhole on top of a slit, (c) the grating and (d) a micrometer screw allowing for adjustment of the light assembly in y direction (see Sec. III B). *Merging and manipulation chamber*: (e) represents the linear manipulator for changing optical bandpass filter and Be x-ray window, (f) the pellicle beam merger and (g) and (h) the first and second retractable optical lenses, respectively. *Bond x-ray spectrometer*: (i) is the first detector and (j) the second one, (k) the crystal, and (l) a glass window for optical alignment.

differ on the level of 2 ppm, our measurements provide benchmarks for these calculations.

We describe the laser-assisted Bond technique, i. e., the combination of the light fiducials with the Bond method in detail, giving special emphasis to the estimate of the accuracies achievable and to the discussion of remaining error contributions.

II. SPECTROMETER ARRANGEMENT

An overview on the measuring setup and its principle is sketched in Fig. 1. The central unit is a Bond precision flat crystal x-ray spectrometer, for details see Fig. 2, designed to measure mirrored Bragg angles θ and $-\theta$ determined by means of two opposed two-dimensional detectors (i) and (j) viewing alternatively the diffracting side of the crystal (k). The detectors (i, j) are simultaneously used also for determining the position of the light fiducials. They can be rotated by $\pm 30^\circ$ by two opposing stepper motor driven flexible bellows. The rotation angles are measured with an uncertainty of $\sim 10^{-3}^\circ$.

One crystal (k) can be mounted on the stepper motor driven crystal holder which can be rotated using a vacuum rotation platform. Its rotation angle ξ is measured with an absolute precision of $5 \times 10^{-5}^\circ$ by means of an incremental angular encoder. For our experiments, this crystal holder was balanced by supporting it from one side to reduce excentric forces acting on the angular encoder. The holder allows for rotation of the crystal around its surface normal, in order to align ϕ , the pivot angle between the crystal surface and the crystal lattice planes, perpendicular to the diffraction plane. Thus, differences in the reference planes for the reflection angles of the x-rays and the light fiducials have been effectively reduced.

The crystal receives simultaneously photons, both from an x-ray source (EBIT) and an angular fiducial visible light source where this source (a) utilizes a well-defined interference pattern from a transmission grating (c) diffracted laser beam (635 nm) for relative angular calibration. Both photon beams are overlaid in a merger and manipulation chamber

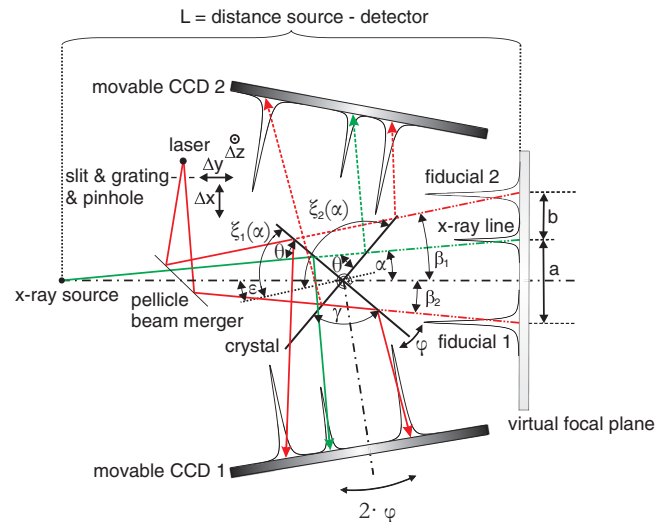


FIG. 2. (Color online) Unification of the light fiducial method and the Bond technique. Here, α and $\beta_{1,2}$ are the angles between the direction from the source to the rotation axis of the crystal and the x-ray, respectively the light fiducial beams, $\xi_1(\alpha)$ and $\xi_2(\alpha)$ the crystal angles determined for $(a/b)_1(\alpha) = (a/b)_2(\alpha) = (a/b)(\alpha)$, where a and b are the distances from the light fiducials to the x-ray line, ϵ the offset angle of the crystal angular measurement, $\gamma = \xi_1(\alpha) - \xi_2(\alpha)$, ϕ an arbitrary crystal rotation and 2ϕ the corresponding detector rotation angle. Δx and Δy characterize shifts in the grating and the ion cloud position. Notice that the order of light fiducials on the CCD detector planes is reversed. The function of the pinhole is described in detail in Sec. III B 2.

TABLE I. Properties of the main components used; three single-crystals were employed. The pivot angles Φ and the orientations of the crystal lattice planes with respect to the crystal rectangular shape long axis (lattice orientation) were measured by the Förster group (Ref. 43).

Device	Model	Properties
Be foil (e)		Thickness: 25 μm Transmission efficiency > 70% ($E_{x\text{-ray}}=2\text{--}8\text{ keV}$)
Beam merger (f)		2 μm nitrocellulose foil X-ray transmission: $\sim 92\%$ Light reflectivity: $\sim 8\%$
Detector (i, j)	Andor (model: CCD42-40)	Back-illuminated, Peltier cooled CCDs Pixel size 13.5 μm^2 Detection area 2048×2048 pixels Quantum efficiency $\sim 100\%$ ($E_{x\text{-ray}} = 0.3\text{--}6\text{ keV}$)
Detector angle Crystals (k)	Heidenhain ERA 880C	Detector angle Φ with $\Delta\Phi < 10^{-3}^\circ$ Si-111, Si-220 and quartz 31- $\bar{4}$ 0 Pivot angles Φ (Ref. 43) 0.0585° , 0.026° , and 0.103° ($\pm 0.002^\circ$) Lattice orientation (Ref. 43) $23.3 \pm 2^\circ$, $40 \pm 4^\circ$, and $15.7 \pm 1^\circ$
Crystal rotation	RP100M Vacuum Generators	0.05° divisions with Vernier (0° to 360°)
Crystal angle	Heidenhain RON 905	Crystal angle ξ with $\Delta\xi < 5 \times 10^{-5}^\circ$

by a light reflecting but x-ray transmitting thin membrane, the pellicle beam merger (f). Within this chamber additionally a manipulator allows for rapid exchange of a bandpass filter (440 nm) and a beryllium foil (e). The Be foil is needed for the x-ray measurements whereas the bandpass filter is used for optical adjustment of the fiducial light source. Both filter and window are compulsory for respective background reduction. At the exit of the merger chamber two retractable lenses (g,h) can be inserted into the beamline in order to focus visible light to the detector plane (see Sec. IV). The characteristic details of the components for our setup can be found in Table I.

The x-ray spectrometer axis, i.e., the rotation axis of the crystal, was mounted parallel (shown in Fig. 1) or perpendicular, i.e., head on, to the electron beam - line or point source, respectively (UHV vacuum 10^{-9} mbar). The distance L between EBIT and spectrometer represents a compromise between photon flux and resolution $\lambda/\Delta\lambda$.

III. MEASUREMENT PRINCIPLE

The laser-assisted Bond technique relies on a precise knowledge of the geometrical parameters of the flat crystal x-ray spectrometer and exploiting light fiducials is crucial. X-rays and laser beams are reflected by the same rotatable flat crystal (k) according to Bragg's law, respectively to the specular optical reflection law, in direction of the CCDs (i, j) (Fig. 2). As discussed in detail in Ref. 3 the incoming directions, α for the x-rays and $\beta_{1,2}$ for the light fiducials, and finally the Bragg angles of the x-rays are then determined by measuring the ratio $a/b(\alpha)$ of the distances $a(\alpha)$ and $b(\alpha)$ from the light fiducial positions to the x-ray line position on the detector plane as a function of the crystal rotation angle $\xi(\alpha)$. Here, the same ratio $a/b(\alpha)$ indicates the same direction for incoming x-rays of different energy. Furthermore, since the theorem on intersecting lines can be applied, the ratio $a/b(\alpha)$

and, thus, the method are both widely insensitive to changes in the crystal or detector positions, as long as the origin of the x-rays and the laser light overlap.³

A. Geometry of the light fiducial setup

As illustrated in Fig. 2, a crystal rotation by $\gamma = 180^\circ - 2\theta = \xi_1(\alpha) - \xi_2(\alpha)$ leads for x-rays of identical incoming directions to be reflected to the respective other detector with equal ratios $a/b(\alpha)$ measured on both CCDs. Here, θ is the Bragg angle of the line of interest and $\xi_1(\alpha)$, $\xi_2(\alpha)$ the crystal angles corresponding to the start and end positions of the crystal rotation, respectively. The ratios $a/b(\alpha)$ are determined as a function of the crystal angle $\xi(\alpha)$, and the resulting curves $a/b(\xi)$ are then used to calculate θ by means of the difference in the crystal angles $\theta = (180^\circ - \xi_1(\alpha) + \xi_2(\alpha))/2$. Here, $\xi_1(\alpha)$ and $\xi_2(\alpha)$ have to be obtained under the constraint that $(a/b)_1(\alpha) = (a/b)_2(\alpha)$, $(a/b)_1(\alpha)$ being the ratio $a/b(\alpha)$ of one detector, and vice versa. Advantageously, while applying this method only the differences in the crystal angles $\xi_1(\alpha) - \xi_2(\alpha)$ are considered in the data analysis and, consequently, a possible offset angle ϵ has no influence on the measured Bragg angle.

B. Alignment of the origin of the light fiducials

In order to achieve a wavelength determination with a total uncertainty of $\Delta\lambda/\lambda \sim 1$ ppm the method described above requires (virtual) spatial overlap of the positions of the adjustable grating, i.e., the origin of the light fiducials, and the ion cloud, i.e., the origin of the x-rays, within certain boundaries Δx and Δy (see Fig. 2).

Using the geometrical relation

$$\frac{a}{b}(f) = \frac{S \cdot \tan(\beta_1) + \Delta y - M}{S \cdot \tan(\beta_2) - \Delta y + M} \quad (1)$$

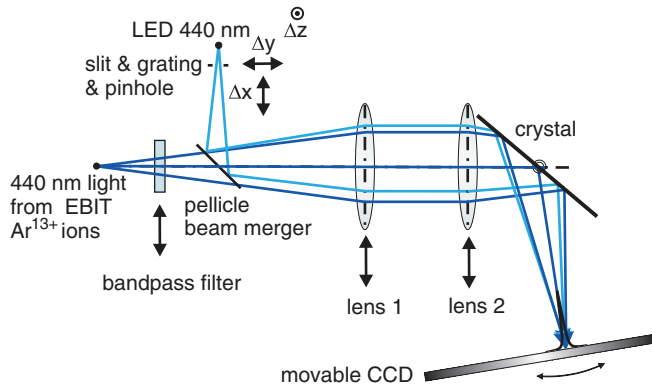


FIG. 3. (Color online) Alignment of the transmission grating. The y positions of the slit, grating and ion cloud are measured by imaging onto the detector plane and projecting their images on the wavelength dispersive detector axis. Overlap is achieved by moving slit and grating correspondingly.

for the ratio a/b in dependence of Δx and Δy , and the definitions $f = (\alpha, \beta_1, \beta_2, \Delta x, \Delta y, L)$, $S = (L - \Delta x)$ and $M = L \cdot \tan(\alpha)$, the former two were calculated to $\Delta x \leq 5$ mm and $\Delta y \leq 0.5$ mm. Here, L refers to the distance between the x-ray source and the detector, α is the angle of the incoming direction for the diffracted x-rays and $\beta_1 + \beta_2$ is the separation angle between the light fiducials, respectively. As expected, alignment in the x direction is less crucial than in the y direction and can be met comparatively easily by carefully mounting the grating. In contrast, for the lateral y direction, a determination of the positions of the ion cloud and the transmission grating and a subsequent sophisticated adjustment of the position of the grating are required.

1. Adjustment in y direction

The position of the cloud is measured by imaging it onto the detector plane. Boron-like argon is produced and trapped in our EBIT. Its $2s^2 2p_{3/2} \rightarrow 2s^2 2p_{1/2}$ forbidden transition is excited by electron impact, and as depicted in Fig. 3 the ~ 440 nm light emitted passes the bandpass filter suppressing stray light and is reflected by the crystal toward the detectors. To measure the position of the grating which is mounted underneath a slit (see also (b) in Fig. 1), this slit is illuminated by a light emitting diode at 440 nm, the light is coupled into the beam path of the x-rays by the pellicle beam merger and reflected by the crystal on the detector plane. During both measurements focussing onto the CCD plane is achieved by two achromatic lenses. The y position of the slit and grating is adjusted to the cloud position by comparing the fitted peak positions of the projections of their images on the wavelength dispersive detector axis and by moving the slit correspondingly using the micrometer screw (d) in Fig. 1. In this way, an overlap in the y position is achieved within $\pm \sim 25 \mu\text{m}$.

2. Corrections for the extended source

The influence of a possible misalignment Δz of the x-ray spectrometer in axial direction, i.e., with respect to a geometry where the centers of the x-ray source, the crystal and the detectors, and the crystal lattice normal lie inside the diffrac-

tion plane, was calculated taking into account that all x-ray lines exhibit a minute curvature in the detector plane (perpendicular to the dispersion plane). Consequently, projecting raw data x-ray peak positions are shifted by an assumed factor K compared to those of ideal straight lines. For the light fiducial method this implies that at equal incoming direction of the x-rays the ratios a/b for both detectors show a reversed behaviour, $a/b(\alpha) = (a/b)_1(\alpha) = (a/b)_2(\alpha)$ being changed to $(a/b)_1(\alpha) = (a + K)/(b - K)$ for the first detector and to $(a/b)_2(\alpha) = (a - K)/(b + K)$ for the second one. The correction angle $\bar{\zeta}$ between the measured Bragg angle θ' determined by projecting curved x-ray lines, and the real Bragg angle θ can be estimated for a misalignment Δz via the relation

$$\bar{\zeta} \approx \arctan \left(\frac{\left(l \left(\frac{q}{2} \right)^3 + q \left(\frac{l}{2} \right)^3 + \frac{3ql}{2} \Delta z^2 \right)}{3L^2 l q} \tan(\theta) \right). \quad (2)$$

Here, L denotes again the distance between the x-ray source and the detector, and q and l are the dimensions of the source and the detector in z direction, respectively. For $L = 1886$ mm, $l = 23$ mm, $\Delta z = 0$, and $q = 40$ mm ($q = 1$ mm) corresponding to a configuration where the x-ray spectrometer axis is mounted parallel (line source) (perpendicular, i.e., head on, (point source)) to the EBIT electron beam the correction angles $\bar{\zeta}$ are on the order of $\sim 10^{-30}$ ($\sim 10^{-40}$). To verify these results, a Monte-Carlo-ray-tracing-simulation which includes all beamline components has been developed. Figure 4 shows the results of this simulation along with the calculated (see Eq. (2)) x-ray reflex for the w -transition in Ar^{16+} including all points along the line source. The graph shows the excellent agreement between this calculation and the simulation.

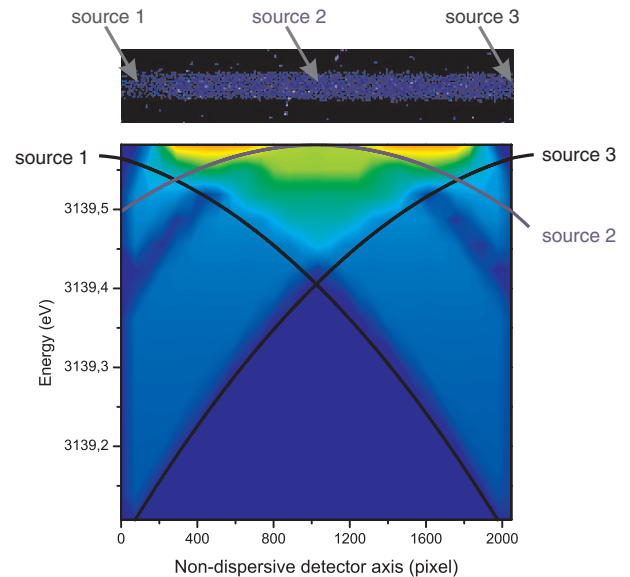


FIG. 4. (Color online) (Top) Image of the ion cloud x-ray source taken with a pinhole camera. (Bottom) Simulated (Monte-Carlo-ray-tracing-simulation) and calculated (see Eq. (2)) x-ray reflex for the w -transition in Ar^{16+} . The x-ray spectrometer was oriented parallel to the EBIT electron beam (line source). While the ray-tracing-simulation includes all point sources (see 2D intensity plot), for the calculation three point sources (see three lines) with $y = 0$ (see Fig. 2) are depicted exemplarily. Sources 1 and 3 represent the point sources at the edges ($\Delta z = \text{maximal}$) of the line source while 2 denotes the central point source ($\Delta z = 0$).

Disregarding the correction angles $\bar{\zeta}$ an unacceptable systematic error of $\Delta\lambda/\lambda \approx 25$ ppm ($\Delta\lambda/\lambda \approx 5$ ppm) is induced in the wavelength determination. Accordingly, in our earlier publication¹² taking this effect only partially into account we stated a larger error of 20 ppm.

3. Adjustment in z direction

To improve the alignment in z direction two approaches have been followed: reducing the line curvature and determining its magnitude experimentally. Minimizing the curvature while at the same time preserving the x-ray flux (which would imply using a point source), requires very good alignment. The z positions of the center of the ion cloud, the crystal and the detectors, as well as of the origin of the light fiducials, have to be measured on an absolute scale with respect to the crystal surface normal and the position of the spectrometer has to be adjusted correspondingly, such that all these points lie inside the diffraction plane, and $\Delta z = 0$.

- The position of the crystal center is determined coupling a He-Ne-laser that is adjustable in the z direction from the back side into the spectrometer main chamber through an UHV window (1 in Fig. 1) opposite of the EBIT port. Its back-reflection from the crystal is monitored as a function of z . This allows to align the beam parallel to the crystal surface normal and to determine the z position of the crystal center.
- The z positions of the CCD centers are measured relatively to the surface normal and the crystal center. The laser is adjusted to the crystal center and the crystal is rotated reflecting the He-Ne-laser on either one of the two CCDs. The z position of the laser spot recorded is compared to the z position of the crystal center. A difference in the two positions is taken into account in the data analysis.
- The z position of the cloud center is measured according to the procedure described for the alignment in Sec. III B 1.
- The z position of the origin of the light fiducials is determined with respect to the diffraction plane and the cloud center. The crystal is rotated in a way that allows for the aligned laser beam to enter the spectrometer beamline. It is reflected by the pellicle beam merger onto the pinhole of the fiducial light source (b in Figs. 1 and 2) whose z position is changed until the laser beam is aligned with it. The laser is switched off and the two retractable lenses are inserted into the beamline. An image of the pinhole, its z position and the trajectories of the diffraction plane at the distance between source and detector L are determined by illuminating the pinhole with 440 nm photons of the light emitting diode and focussing the light on the detector plane. The pinhole is removed after establishing alignment.

The difference in the z position of the crystal and the ion cloud center relative to the diffraction plane is corrected for by shifting the spectrometer correspondingly. The z position of the origin of the light fiducials is changed by adjusting the laser beam generating the light fiducials to the z position of

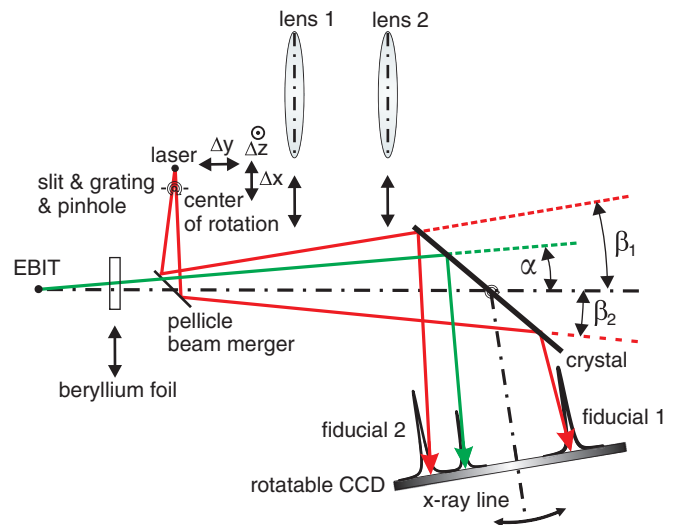


FIG. 5. (Color online) Generation of the light fiducials. Their separation angles of $\beta_{1,2} \sim 0.15^\circ$ can be changed to $\beta_1 = \beta_2$ by rotating the light fiducial assembly in the x - y -plane.

the pinhole. We estimate that the remaining deviation from the ideal spectrometer configuration together with the fact that the setup was adjusted to the crystal surface rather than to the lattice normal, both lead to a maximum uncertainty of ~ 0.3 ppm in the determination of the x-ray transition energy. This error contribution is denoted as “fiducials” in Sec. IV B.

After alignment in Δx , Δy , and Δz directions, the lenses are retracted for the remaining measurement period, and the light fiducials are generated (see Fig. 5). Their incoming angles of $\beta_{1,2} \sim 0.15^\circ$, corresponding to a grating constant of $g = 0.2$ mm, can be adjusted to $\beta_1 = \beta_2$ by rotating the light fiducial assembly in the x - y -plane. The slit is placed at the center of rotation, thus preserving the established alignment.

4. X-ray line profiles

Moreover the x-ray line curvature was observed experimentally. X-ray sum spectra (see Fig. 6) were carefully analyzed, determining the position of the x-ray peak on the wavelength dispersive axis as a function of the position on the non-dispersive axis (slices). The results are depicted in Fig. 7 for the w -transition in Ar^{16+} measured with the x-ray spectrometer rotation axis oriented parallel to the electron beam (line source). Excellent agreement between this observations and a simulated curvature calculated using the Monte-Carlo-ray-tracing-simulation described above is found. The magnitude of the curvature could be obtained with an uncertainty of about $\sim 6.5 \times 10^{-5}^\circ$ corresponding to an error contribution on the order of ~ 1.3 ppm in the wavelength determination, which is listed as “curvature” in Sec. IV B. As a result and compared to our earlier measurements¹² the contribution of the line curvature on the detectors to the total absolute error budget has been reduced by more than a factor 10 for this spectrometer configuration.

IV. DATA ANALYSIS AND RESULTS

A detailed description of the EBIT settings, measurement procedure, data acquisition and analysis can be found in Ref. 3.

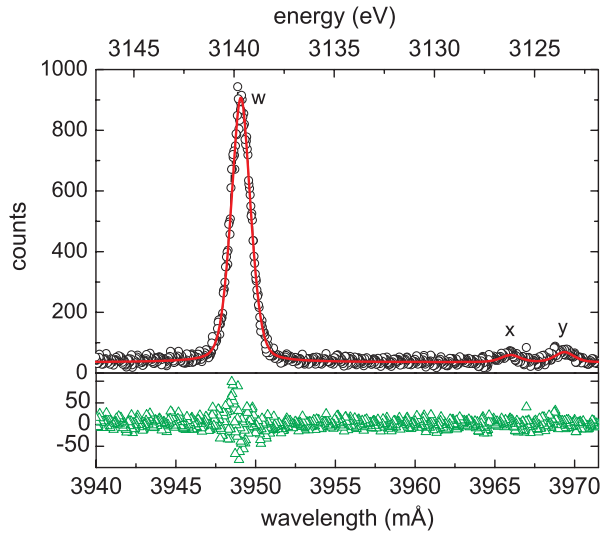


FIG. 6. (Color online) Experimental sum spectrum (black dots) of the w ($1s2p^1P_1 \rightarrow 1s^2^1S_0$), x ($1s2p^3P_2 \rightarrow 1s^2^1S_0$) and y ($1s2p^3P_1 \rightarrow 1s^2^1S_0$) transitions in Ar^{16+} with Voigt fit (red line) and residuum (light green triangles) at the bottom.

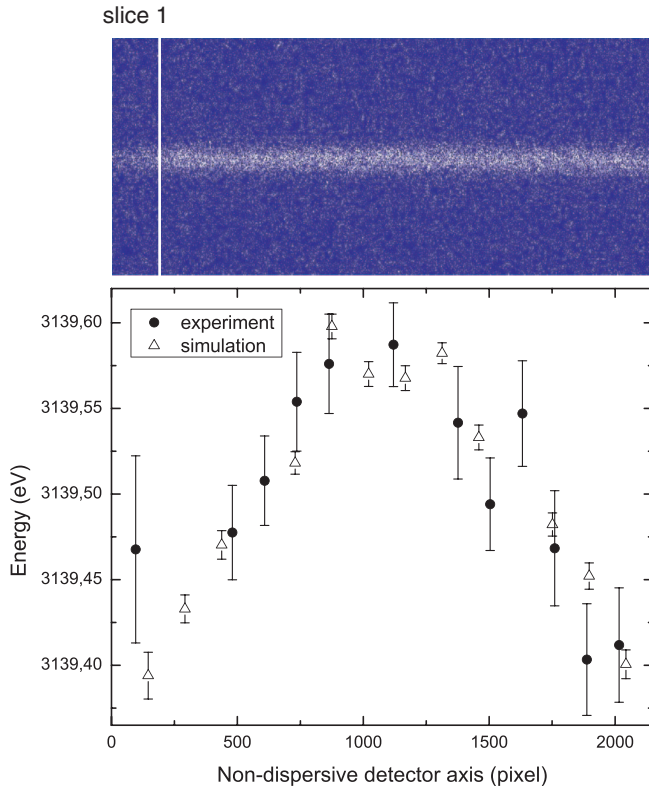


FIG. 7. (Color online) (Top) X-ray sum spectrum for the w -transition in Ar^{16+} . (Bottom) Measured x-ray energy as a function of the position on the non-dispersive axis (slices). The latter is binned 32 times. X-ray energies were calculated by determining the peak maxima through Voigt fits on the experimental (dots) and simulated (Monte-Carlo-ray-tracing-simulation; triangles) line profiles. These were obtained by projecting the x-ray sum spectrum on the dispersive axis. The whole process was automated and only data points which could be fitted by the program in a reasonable number of iterations are displayed. The x-ray sum spectrum was measured with the x-ray spectrometer axis mounted parallel to the EBIT electron beam.

Here, we want to discuss mainly crucial changes in the data analysis, sources of systematic errors, and their influence on the total uncertainty of wavelength measurements while using the laser-assisted Bond method as well as the results of our latest experiments on the w -transition in Ar^{16+} .

A. Determination of the Bragg angle and the wavelength of the w -transition

The ratios $a/b(\alpha)$ for the w -line are plotted for both detectors as a function of the measured crystal angle ξ . Both curves are fitted according to the procedure described in Ref. 3. The two detector crystal angles $\xi_1(\alpha)$ and $\xi_2(\alpha)$ are obtained at equal ratios $a/b(\alpha)$ of the x-ray line. The Bragg angle θ' is calculated via the relation $\theta' = (180^\circ - \xi_1(\alpha) + \xi_2(\alpha))/2$ (see Sec. III A). However, the effect of the x-ray line curvature on the measured Bragg angle θ' has to be considered. Therefore, two approaches are followed. In a first ansatz, the correction angle $\tilde{\zeta}$ (see Sec. III B 2) is determined by calculating the average value of the absolute peak positions of the fits to the curved x-ray line profiles for all positions on the non-dispersive axis (see Fig. 7). The real Bragg angles θ are then obtained correcting the measured Bragg angles θ' according to the relation $\tilde{\zeta} = \theta' - \theta$. In a second approach, the experimental data is fitted using the equation for the shift of the peak position on the wavelength dispersive axis as a function of the position on the non-dispersive axis. The curved x-ray line is transformed into an ideal straight line shifting each row of the non-dispersive axis corresponding to the fit results parallel to the dispersive axis. Both approaches yielded consistent results for the real Bragg angle θ . This angle is converted into wavelength via the relation

$$\lambda = 2d \sin(\theta) \left(1 - \frac{\delta_\lambda}{\sin^2(\theta)} \right), \quad (3)$$

with δ_λ being the refractive index of the Si-111 crystal at the wavelength λ and d its lattice constant. The former is taken from the Center for X-Ray Optics⁴⁴ while the latter is determined to be $2d = 6.271\,219(3) \text{ \AA}$ using the values $2d = 6.27\,120\,246(16) \text{ \AA}$ and $2.60 \times 10^{-6} \text{ K}^{-1}$ temperature for the Si-111 lattice constant and the linear temperature coefficient of expansion of silicon, respectively, as recommended for vacuum conditions and 22.5°C by CODATA.³⁸ Finally, the transition energy is calculated from the wavelength determined to be $3949.068(6) \text{ m\AA}$ for the w -line in He-like Ar^{16+} setting the wavelength-to-energy conversion factor to $hc = 1.239\,841\,875 \times 10^{-6} \text{ eV m}$ yielding a transition energy of $3139.581(5) \text{ eV}$.

B. Error budget

Table II shows the remaining error contributions for the w -transition wavelength in Ar^{16+} after alignment and temperature stabilization of the spectrometer setup. Here, “fiducials” refer to the error caused by the remaining uncertainty in the position of the origin of the light fiducials after alignment to the origin of the x-rays. “Curvature” takes into account the uncertainty of about $6.5 \times 10^{-5}^\circ$ in the determination of the correction angle $\tilde{\zeta}$ for a configuration where

TABLE II. Total error budget of our energy determination on the w -transition in Ar^{16+} . The spectrometer main axis was oriented parallel to the EBIT electron beam.

Error source	Abs. uncertainty (meV)	Rel. uncertainty (ppm)
Statistics	~ 0.5	~ 0.2
Lattice	~ 2.5	~ 0.8
Curvature	~ 4.0	~ 1.3
Fiducials	~ 1.0	~ 0.3
Total	~ 4.8	~ 1.5

the x-ray spectrometer rotation main axis is oriented parallel to the EBIT electron beam. “Lattice” is related to the contribution induced by minor fluctuations $\Delta T < 0.3$ K in the temperature of the experimental area which lead to variations of about 3×10^{-6} Å in the crystal lattice constant and, thus, to an uncertainty of about 3×10^{-5} eV in the determination of the Bragg angles. Finally, “statistics” accounts for the limited counting statistics. It can be seen that the total error of the wavelength measurement on the w -transition in Ar^{16+} is dominated by the ± 2.5 meV and ± 4.0 meV contribution of the uncertainty in the lattice constant and in the curvature of the x-ray lines, respectively. However, in recent experimental tests the latter contribution could be reduced additionally by up to a factor of ~ 25 mounting the spectrometer axis perpendicular to the EBIT electron beam axis by looking head on to the ion cloud through the electron collector aperture (x-ray point source). This minimizes the dimension q of the x-ray source in z direction and, consequently, the line curvature (Eq. (2)). Apart from that, in future measurements the contribution “lattice” will be diminished further if the temperature of the spectrometer setup can be stabilized to $\Delta T \ll 0.3$ K.

C. Results and discussion

Our measurements on the w -line in Ar^{16+} yields a transition energy of 3139.581(5) eV or a wavelength of 3949.068(6) mÅ with an error of 1.5 ppm only. Figure 8 compares this result with former experimental values^{3,9,12} and theoretical predictions.^{45–47} Regarding the experimental results it has to be emphasized that in our 2005,³ 2007,¹² and the Deslattes *et al.*⁹ experiment the wavelength of the w -line was determined relatively to the Lyman- α lines of Ar^{17+} with only the present experimental values being obtained through absolute wavelength measurements. Besides, an important point is that for our first high-precision measurement on this line in 2005 the origin of the light fiducials was not aligned in x and y direction with the origin of the x-rays. Unfortunately, this was not considered in the error analysis such that the total uncertainty for the 2005 result is underestimated. We want to indicate as well that in our 2007 experiment¹² a final uncertainty of the absolute wavelength measurements of roughly 20 ppm could not be excluded. This figure could be significantly reduced by correcting the curvature of the x-ray lines in the detector plane comparing the theoretical and absolutely measured values for the wavelength of the Lyman- α_1 line in Ar^{17+} , attributing a possible deviation to the curvature and scaling the effect to the wavelength of the w -line.

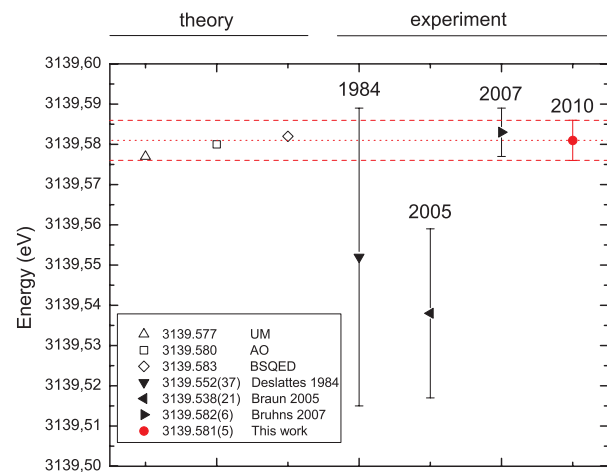


FIG. 8. (Color online) Comparison of our present result (red) with other experimental and theoretical values for the w -line in Ar^{16+} . Theory: UM unified method;⁴⁵ AO all-order;⁴⁶ BSQED.⁴⁷ Experiment: Deslattes *et al.*,⁹ Braun *et al.*,³ Bruhns *et al.*¹² The present total uncertainty of 4.8 meV is indicated by the dashed lines.

In contrast, in the present measurements the curvature was determined explicitly, and an extensive simulation of this effect was carried out. In summary, aligning the origin of the light fiducials with respect to the origin of the x-rays in x and y direction, providing an absolute instead of a relative wavelength measurement and exactly adjusting the spectrometer setup in z direction the total experimental uncertainty could be reduced by a factor of 10 between 2005 and today. Thus, the current result, the only absolute, reference-line free measurement on this line, represents the most precise value for a wavelength of any He-like ion reported so far, being a factor 1.2 more accurate than the previous best relative result¹² provided also by our group.

We want to emphasize that our 2007 and the latest experimental value agree within <1 ppm in spite of the fact that the spectrometer assembly was dismantled and rebuilt several times in between these measurements. This demonstrates the outstanding reproducibility of our results when using the laser-assisted measurement method. In contrast, a comparison with the previous result by Deslattes *et al.*⁹ shows a slight discrepancy of the absolute values, even though that within uncertainties overlap is achieved. However, in the latter experiment Ar^{16+} ions were produced as recoil ions in a gas cell by collisions with fast highly charged uranium ions. As stated by the authors contamination of the spectra with satellite lines is likely and could have led to a shift in the x-ray line centroid and a reduction of the measured energy.

Comparing our present result with predictions, it can be stated that it agrees excellently with both the values of bound state QED (BSQED) (Ref. 47) and All Order (AO) (Ref. 46) calculations. In contrast, the result calculated by the unified method (UM) (Ref. 45) deviates by about one standard deviation. This small difference could be explained by the fact that UM does not include higher order relativistic corrections to the electron-electron interaction, and could indicate that already for He-like systems with nuclear charge $Z = 18$ relativistic effects play an important role in the calculations of the QED contributions to the energy levels. Table III shows

TABLE III. Theoretical one- and two-electron QED contributions (in eV) to the $1s2p\ ^1P_1$ and $1s^2\ ^1S_0$ states in Ar^{16+} (BSQED) (Ref. 47). Total 1-el.: sum of one-electron terms; Scr. SE: screened self-energy; Scr. VP: screened vacuum polarization; 2-ph. exch.: exchange of two virtual photons; total 2-el.: sum of two-electron terms.

State	Total 1-el.	Scr. SE	Scr. VP	2-ph. exch.	Total 2-el.
1S_0	-1.1310	0.1116	-0.0072	-0.0091	0.0953
1P_1	-0.0062	0.0031	-0.0001	0.0001	0.0031

the theoretical one- and two-electron QED terms⁴⁷ of the $1s2p\ ^1P_1$ excited and $1s^2\ ^1S_0$ ground states of Ar^{16+} , respectively. The uncertainty of our present result is a factor of ~ 20 smaller than all of the two-electron QED corrections to the 1S_0 ground state energy and a factor of 2 smaller than the corrections caused by the exchange of two virtual photons (9 meV). Consequently, the experiment probes these QED contributions as well as the total one-electron contribution of the excited 1P_1 state (6 meV) but is not yet sensitive to its total two-electron term (3 meV).

We finally want to mention that future measurements will focus on He-like transitions of other elements, probing QED over its whole range from the regime where calculations are dominated more by electron-electron interactions to the highly relativistic domain. Besides, using our laser-assisted method, x-ray line energies of other systems, e.g., hydrogen-like ions, can be absolutely determined with uncertainties as small as 1 ppm. This could allow to establish Lyman- α lines of H-like ions as future atomic x-ray standards, e.g., for the calibration of microcalorimeters or for resonant laser excitation experiments at third generation synchrotrons and free-electron lasers (FEL).^{23,24} Finally, in this context it seems promising to use the here presented spectrometer setup for high-precision FEL x-ray emission spectroscopy.

- ¹H. G. J. Moseley, *Philos. Mag.* **26**, 1024 (1913).
- ²H. G. J. Moseley, *Philos. Mag.* **27**, 703 (1914).
- ³J. Braun, H. Bruhns, M. Trinczek, J. R. Crespo López-Urrutia, and J. Ullrich, *Rev. Sci. Instrum.* **76**, 073105 (2005).
- ⁴M. A. Levine, R. E. Marrs, J. R. Henderson, D. A. Knapp, and M. B. Schneider, *Phys. Scr.* **22**, 157 (1988).
- ⁵M. A. Levine, R. E. Marrs, J. N. Bardsley, P. Beiersdorfer, C. L. Bennett, M. H. Chen, T. Cowan, D. Dietrich, J. R. Henderson, D. A. Knapp, A. Osterheld, B. M. Penetrante, M. B. Schneider, and J. H. Scofield, *Nucl. Instrum. Methods B* **43**, 431 (1989).
- ⁶K. Widmann, P. Beiersdorfer, J. R. Crespo López-Urrutia, and S. R. Elliott, *Hyperfine Interact.* **108**, 73 (1997).
- ⁷J. R. Crespo López-Urrutia, B. Bapat, B. Feuerstein, D. Fischer, H. Lörch, R. Moshhammer, and J. Ullrich, *Hyperfine Interact.* **146**, 109 (2003).
- ⁸H. F. Beyer, R. D. Deslattes, F. Folkmann, and R. E. LaVilla, *J. Phys. B* **18**, 207 (1985).
- ⁹R. Deslattes, H. Beyer, and F. Folkmann, *J. Phys. B* **17**, L689 (1984).
- ¹⁰H. Beyer, P. Indelicato, K. Finlayson, D. Liesen, and R. D. Deslattes, *Phys. Rev. A* **43**, 223 (1991).
- ¹¹E. S. Marmar, J. E. Rice, E. Källne, J. Källne, and R. E. LaVilla, *Phys. Rev. A* **33**, 774 (1986).
- ¹²H. Bruhns, J. Braun, K. Kubiček, J. Crespo López-Urrutia, and J. Ullrich, *Phys. Rev. Lett.* **99**, 113001 (2007).
- ¹³R. Marrs, S. Elliott, and T. Stöhlker, *Phys. Rev. A* **52**, 3577 (1995).
- ¹⁴G. Y. Liang, J. R. Crespo López-Urrutia, T. M. Baumann, S. W. Epp, A. Gonchar, A. Lapiere, P. H. Mokler, M. C. Simon, H. Tawara, V. Mäkel, K. Yao, G. Zhao, Y. Zou, and J. Ullrich, *Astrophys. J.* **702**, 838 (2009).
- ¹⁵M. R. Tarbutt, D. Crosby, E. G. Myers, N. Nakamura, S. Ohtani, and J. D. Silver, *The Hydrogen Atom*, (Springer, New York, 2001), Vol. 570, pp. 727–736.
- ¹⁶C. T. Chantler, D. Paterson, L. T. Hudson, F. G. Serpa, J. D. Gillaspay, and R. D. Deslattes, *Phys. Scr.* **73**, 87 (1997).
- ¹⁷R. S. Orts, J. R. Crespo López-Urrutia, H. Bruhns, A. J. González Martínez, Z. Harman, U. D. Jentschura, C. H. Keitel, A. Lapiere, H. Tawara, I. I. Tupitsyn, J. Ullrich, and A. V. Volotka, *Phys. Rev. A* **76**, 052501 (2007).
- ¹⁸J. Xiao, Y. Gao, X. Zhang, D. Lu, W. Hu, M. Gao, W. Chen, and Y. Zou, *Rev. Sci. Instrum.* **79**, 093101 (2008).
- ¹⁹M. Niering, R. Holzwarth, J. Reichert, P. Pokasov, T. Udem, M. Weitz, T. W. Hänsch, P. Lemonde, G. Santarelli, M. Abgrall, P. Laurent, C. Salomon, and A. Clairon, *Phys. Rev. Lett.* **84**, 5496 (2000).
- ²⁰M. Fischer, N. Kolachevsky, M. Zimmermann, R. Holzwarth, T. Udem, T. Hänsch, M. Abgrall, J. Grünert, I. Maksimovic, S. Bize, H. Marion, F. Pereira Dos Santos, P. Lemonde, G. Santarelli, P. Laurent, A. Clairon, C. Salomon, M. Haas, U. D. Jentschura, and C. H. Keitel, *Phys. Rev. Lett.* **92**, 230802 (2004).
- ²¹V. Mäkel, R. Klawitter, G. Brenner, J. R. Crespo López-Urrutia, and J. Ullrich, *Phys. Rev. Lett.* **107**, 143002 (2011).
- ²²See <http://lcls.slac.stanford.edu/instruments.aspx> for technical information on the available instruments; <http://www.xfel.eu/> for current status of the XFEL project; see <http://www.xfel.spring8.or.jp/> for new information on the latest technical upgrades.
- ²³S. W. Epp, J. R. Crespo López-Urrutia, G. Brenner, V. Mäkel, P. H. Mokler, R. Treusch, M. Kuhlmann, M. V. Yurkov, J. Feldhaus, J. R. Schneider, M. Wellhöfer, M. Martins, W. Wurth, and J. Ullrich, *Phys. Rev. Lett.* **98**, 183001 (2007).
- ²⁴S. Bernitt, (unpublished).
- ²⁵“The European x-ray free-electron laser technical design report”, Tech. Rep. (DESY XFEL Project Group European XFEL Project Team Deutsches Elektronen-Synchrotron Member of the Helmholtz Association, Hamburg, Germany; see <http://www.xfel.net>, July 2007).
- ²⁶“Linac coherent light source (lcls) conceptual design report”, Tech. Rep. (Stanford Linear Accelerator Center, Stanford University, Lawrence Livermore National Laboratory, University of California, Argonne National Laboratory, University of Chicago, April 2002).
- ²⁷“Xfel/spring-8 beamline technical design report ver. 2.0”, Tech. Rep. (Spring-8 Joint Project for XFEL Experimental Facility Group, February, 2010).
- ²⁸A. Fleischmann, C. Enss, and G. M. Seidel, *Cryogenic Particle Detection* (Springer, New York, 2005), p. 151.
- ²⁹C. Enss and D. McCammon, *J. Low Temp. Phys.* **151**, 5 (2008).
- ³⁰L. Fleischmann, M. Linck, A. Burck, C. Domesle, S. Kempf, M. Rodrigues, A. Pabinger, C. Pies, J.-P. Porst, H. Rotzinger, S. Schäfer, R. Weldle, A. Fleischmann, C. Enss, and G. M. Seidel, *J. Phys. Conf. Ser.* **150**, 012013 (2009).
- ³¹S. R. Bandler, C. N. Bailey, J. A. Bookbinder, E. E. DeLuca, J. A. Chervenak, M. E. Eckart, F. M. Finkbeiner, D. P. Kelley, R. L. Kelley, C. A. Kilbourne, F. S. Porter, J. E. Sadleira, S. J. Smith, and R. K. Smith, *Proc. SPIE* **7732**, 773238 (2010).
- ³²P. Beiersdorfer, G. V. Brown, J. Clementson, J. Dunn, K. Morris, E. Wang, R. L. Kelley, C. A. Kilbourne, F. S. Porter, M. Bitter, R. Feder, K. W. Hill, D. Johnson, and R. Barnsley, *Rev. Sci. Instrum.* **81**, 10E323 (2010).
- ³³H. H. Johann, *Z. Phys.* **69**, 185 (1931).
- ³⁴L. von Hámos, *Ann. Phys.* **17**(5), 716 (1933).
- ³⁵L. von Hámos, *Ann. Phys.* **19**(5), 253 (1934).
- ³⁶J. W. M. DuMond, *Rev. Sci. Instrum.* **18**, 626 (1947).
- ³⁷R. Deslattes, *J. Res. Natl. Inst. Stand. Technol.* **105**, 1 (2000).
- ³⁸P. J. Mohr, B. N. Taylor, and D. B. Newell, *Rev. Mod. Phys.* **80**, 633 (2008).
- ³⁹N. Nakamura, *Rev. Sci. Instrum.* **71**, 4065 (2000).
- ⁴⁰D. Klöpfel, G. Hölzer, E. Förster, and P. Beiersdorfer, *Rev. Sci. Instrum.* **68**, 3669 (1997).
- ⁴¹W. L. Bond, *Acta Crystallogr.* **13**, 814 (1960).
- ⁴²A. H. Gabriel, *Mon. Not. R. Astron. Soc.* **160**, 99 (1972).
- ⁴³E. Förster, “x-ray optics group of the university of Jena,” see <http://www.physik.uni-jena.de/inst/xro>.
- ⁴⁴Center for X-Ray Optics and Advanced Light Source, see <http://www-cxro.lbl.gov/>.
- ⁴⁵G. W. F. Drake, *Can. J. Phys.* **66**, 586 (1988).
- ⁴⁶D. R. Plante, W. R. Johnson, and J. Sapirstein, *Phys. Rev. A* **49**, 3519 (1994).
- ⁴⁷A. N. Artemyev, V. M. Shabaev, V. A. Yerokhin, G. Plunien, and G. Soff, *Phys. Rev. A* **71**, 062104 (2005).